Interlayer Aharonov-Bohm Interference in Tilted Magnetic Fields in Quasi-One-Dimensional Organic Conductors

Benjamin K. Cooper and Victor M. Yakovenko

Condensed Matter Theory Center and Center for Superconductivity Research, Department of Physics, University of Maryland, College Park, Maryland 20742-4111, USA

(Received 1 September 2005; published 23 January 2006)

Different types of angular magnetoresistance oscillations in quasi-one-dimensional layered materials, such as organic conductors $(TMTSF)_2X$, are explained in terms of Aharonov-Bohm interference in interlayer electron tunneling. A two-parameter pattern of oscillations for generic orientations of a magnetic field is visualized and compared to the experimental data. Connections with angular magnetoresistance oscillations in other layered materials are discussed.

DOI: 10.1103/PhysRevLett.96.037001 PACS numbers: 74.70.Kn, 72.15.Gd, 73.21.Ac

Angular magnetoresistance oscillations (AMRO), where resistivity oscillates as a function of the magnetic field orientation, were originally discovered [1,2] in the quasi-two-dimensional (Q2D) organic conductors of the $(BEDT\text{-}TTF)_2X$ family [3]. AMRO are distinct from the Shubnikov–de Haas and de Haas–van Alphen oscillations and are now widely used for direct mapping of the Fermi surfaces of layered materials [4,5]. AMRO have been observed not only in many organic conductors, but also in intercalated graphite [6], Sr_2RuO_4 [7], $Tl_2Ba_2CuO_6$ [8,9], and GaAs/AlGaAs superlattices [10]. Early theories of AMRO [4,11,12] were formulated in terms of semiclassical electron trajectories on a cylindrical 3D Fermi surface. Then it was realized that AMRO can exist already for two layers [13–15], and they represent an Aharonov-Bohm interference effect in interlayer tunneling [16]. Some experimental evidence for AMRO in semiconducting bilayers has been found [17], but more systematic measurements are necessary.

AMRO were also found in quasi-one-dimensional (Q1D) organic conductors with open Fermi surfaces, such as $(TMTSF)_2X$ [3]. These materials consist of parallel chains along the x axis, which form layers with the interlayer spacing d along the z axis and the interchain spacing b along the y axis, as shown in Fig. 1(a). Originally, three different AMRO were discovered in the Q1D conductors: the Lebed magic angles [18–21] for a magnetic field rotation in the (y, z) plane; the Danner, Kang, and Chaikin (DKC) oscillations in the (x, z) plane [22,23]; and the third angular effect in the (x, y) plane [24–26]. Then Lee and Naughton [27] found combinations of all three effects for generic magnetic field rotations. It became clear that all types of AMRO in Q1D conductors have a common origin and should be explained by a single unified theory.

In $(TMTSF)_2X$, the in-plane tunneling amplitude between the chains, $t_b \sim 250$ K [22,23], is much greater than the interplane tunneling amplitude $t_c \sim 10$ K [3]. Thus, we can treat interlayer tunneling as a perturbation and study the interlayer conductivity σ_c between just two layers for a tilted magnetic field $\boldsymbol{B} = (B_x, B_y, B_z)$, as shown in Fig. 1(a). This bilayer approach [14,15] only assumes phase memory of interlayer tunneling within a decoherence time τ and does not require a well-defined momentum k_z and a coherent 3D Fermi surface. It gives a simple and transparent interpretation of the most general Lee-Naughton oscillations [27] in terms of Aharonov-Bohm interference in interlayer tunneling. The results are equivalent to other approaches based on the classical Boltzmann equation [25–29] and the quantum Kubo formula [30–32]. We calculate contour plots of σ_c as a function of two ratios B_x/B_z and B_y/B_z for models with one or several interlayer tunneling amplitudes [30,33]. This type of visualization clearly reveals agreement and disagreement between theory and experiment and allows us to determine the electronic parameters of the Q1D materials. The results can be also applied to Q1D semiconducting bilayers consisting of quantum wires induced by an array parallel gates, as shown in Fig. 1(a).

Let us consider tunneling between two Q1D layers. The in-plane electron dispersion is

$$\varepsilon(k_x, k_y) = \pm v_F k_x - 2t_b \cos(k_y b/\hbar), \tag{1}$$

where energy ε is measured from the Fermi energy, $\pm v_F$ are the Fermi velocities on the opposite sheets of the open Fermi surface, $\boldsymbol{k} = (k_x, k_y)$ is the in-plane momentum, and

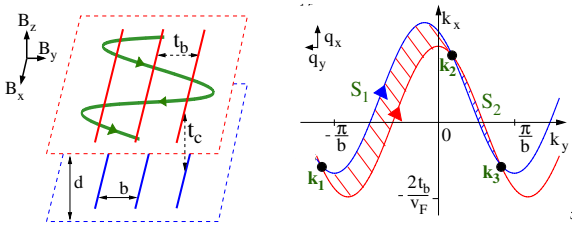

FIG. 1 (color online). (a) Geometry of electron tunneling between two Q1D layers. The sinusoidal line represents the in-plane electron trajectory; t_b and t_c are the amplitudes of interchain tunneling. (b) The Fermi surfaces of the two layers, shifted by the vector $\boldsymbol{q}$ in Eq. (9). The shaded areas S_1 and S_2 lead to interference oscillation in the presence of B_z.

k_x is measured from the Fermi momentum. The interlayer tunneling is described by the Hamiltonian

$$\hat{H}_\perp = t_c \int \hat{\psi}_2^\dagger(\boldsymbol{r})\hat{\psi}_1(\boldsymbol{r})e^{i\phi(\boldsymbol{r})}d^2r + \text{H.c.}, \qquad (2)$$

$$\phi(\boldsymbol{r}) = \frac{ed}{\hbar c}A_z(\boldsymbol{r}), \qquad A_z(\boldsymbol{r}) = B_x y - B_y x, \qquad (3)$$

where $\boldsymbol{r} = (x, y)$, c is the speed of light, e is the electron charge, A_z is the vector potential, and $\hat{\psi}_{1,2}$ are the electron destruction operators in the layers 1 and 2. The gauge phase $\phi(\boldsymbol{r})$ is due to the in-plane magnetic field.

We treat the in-plane electron motion quasiclassically. For $B_z \neq 0$, electrons move in time t along sinusoidal trajectories [34], as shown in Fig. 1(a),

$$x(t) = x_0 \pm v_F t, \qquad y(t) = y_0 \pm \left(\frac{2t_b c}{e v_F B_z}\right)\cos(\omega_c t). \qquad (4)$$

Instead of the magnetic field components (B_x, B_y, B_z), it is convenient to introduce the variables ω_c, B_x', and B_y' defined by the following relations

$$\omega_c = \frac{eb v_F B_z}{\hbar c}, \qquad B_x' = \frac{B_x}{B_z}\frac{2t_b d}{\hbar v_F}, \qquad B_y' = \frac{B_y}{B_z}\frac{d}{b}. \qquad (5)$$

The cyclotron frequency ω_c is simply proportional to B_z, whereas the dimensionless variables B_x' and B_y' are proportional to the ratios of the magnetic field components $B_x/B_z = \cos\varphi\tan\theta$ and $B_y/B_z = \sin\varphi\tan\theta$. Although these ratios can be expressed in terms of the spherical angles θ and φ, we believe that presentation and visualization of the results using B_x' and B_y' is simpler and more insightful than in the spherical angles [15,25,28].

The gauge phase (3) in Eq. (2) leads to interference between interlayer tunneling amplitudes $t_c e^{i\phi(\boldsymbol{r})}$ along the trajectory $\boldsymbol{r}(t)$. In Eq. (4), $y(t)$ oscillates with the period $\Delta t = 2\pi/\omega_c$, whereas $x(t)$ steadily increases, accumulating the phase $\Delta\phi = edB_y v_F \Delta t/\hbar c$ over one period. The average $\langle e^{i\phi(t)}\rangle_t$ vanishes unless $\Delta\phi = 2\pi n$, where n is an integer. This condition selects the Lebed magic angles $B_y' = n$ [18], which in the spherical coordinates are $\sin\varphi = n(b/d)\cot\theta$ [27]. Using Eqs. (3)–(5), we find the effective interlayer tunneling amplitude $\tilde{t}_c$

$$\tilde{t}_c = t_c\langle e^{i\phi(t)}\rangle_t = t_c J_n(B_x') \quad \text{for } B_y' = n, \qquad (6)$$

where J_n is the Bessel function.

AMRO result from a periodic modulation of the effective interlayer coupling $\tilde{t}_c$ in Eq. (6) due to interlayer Aharonov-Bohm interference. The condition $B_y' = n$ requires that the flux of B_y through the area, formed by the interlayer distance d and the electron trajectory period $\Delta x = v_F\Delta t$, is $n\Phi_0$, where $\Phi_0 = hc/e$ is the flux quantum. In addition, $\tilde{t}_c^2$ (6) oscillates as a function of B_x' with the period $\Delta B_x' = \pi$. These DKC oscillations [22] are related to the flux of B_x through the area bounded by d and $\Delta y = 4t_b c/e v_F B_z$, the transverse width of the electron trajectory in Eq. (4). More precisely, it is necessary to consider the distance between the turning points of an electron trajectory, as viewed along the vector (B_x, B_y). This will be discussed in more detail from the momentum-space point of view.

The interlayer ac conductivity $\sigma_c(\omega)$ is given by a correlator of tunneling events at times t and t' [14,15]

$$\sigma_c(\omega) \propto \mathcal{R}e\, t_c^2\langle \int_t^\infty e^{i\phi(t')-i\phi(t)}e^{(t'-t)(i\omega-1/\tau)}dt'\rangle_t, \qquad (7)$$

where τ is a relaxation time. Substituting Eqs. (3) and (4) in Eq. (7), we find

$$\frac{\sigma_c(\boldsymbol{B},\omega)}{\sigma_c(0,0)} = \sum_{n=-\infty}^{\infty}\frac{J_n^2(B_x')}{1+(\omega_c\tau)^2(n-B_y'\mp\omega/\omega_c)^2}, \qquad (8)$$

where $\sigma_c(0,0)$ is the dc conductivity at $\boldsymbol{B} = 0$, and the signs $\mp$ in the denominator originate from the $\pm v_F$ sheets of the Fermi surface. Equation (8) is in agreement with Refs. [12,14,15,30,31]. It can be applied to the microwave measurements at $\omega \neq 0$ [35,36], but below we concentrate on the dc case $\omega = 0$. When $\omega_c\tau \to \infty$, only the term with $n = B_y'$ survives, and Eq. (8) reduces to $\sigma_c(\boldsymbol{B},0)/\sigma_c(0,0) = (\tilde{t}_c/t_c)^2$ with $\tilde{t}_c$ from Eq. (6). In Fig. 2, we show the contour plot of $\sigma_c(\boldsymbol{B},0)/\sigma_c(0,0)$ vs B_x' and B_y' calculated from Eq. (8) for $\omega_c\tau = \sqrt{50} \approx 7.1$. The dc conductivity σ_c is maximal at the vertical stripes, labeled by the integer numbers n, which correspond to the Lebed magic angles $B_y' = n$. Within the nth vertical stripe, σ_c has alternating maxima and minima, indicated by circles and squares, which represent oscillations of J_n^2 vs B_x' in Eqs. (6) and (8). Positions of these maxima and minima can be obtained from the Aharonov-Bohm interference in momentum space, as described below.

Eqs. (2) and (3) show that, in the process of interlayer tunneling, the in-plane electron momentum changes by

$$\boldsymbol{q} = (q_x, q_y) = (ed/c)(B_y, -B_x). \qquad (9)$$

Thus, the Fermi surfaces of the two layers are displaced relative to each other by the vector $\boldsymbol{q}$ [14,15], as shown in

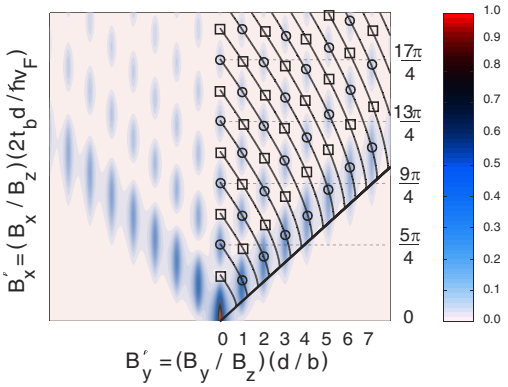

FIG. 2 (color online). The contour plot of angular oscillations in the normalized interlayer dc conductivity $\sigma_c(\boldsymbol{B},0)/\sigma_c(0,0)$, Eq. (8). The variables B_x' and B_y' are defined in Eq. (5). The lines with circles and squares indicate where interference between the two trajectories in Fig. 1(b) is constructive and destructive.

Fig. 1(b). Electrons can tunnel between the layers only at the intersection points $\boldsymbol{k}_1$, $\boldsymbol{k}_2$, $\boldsymbol{k}_3$, etc., of the two Fermi surfaces, where the conservation laws of energy and momentum are satisfied. In the presence of B_z, there is a phase difference between the two trajectories connecting the intersection points, which is proportional to the shaded momentum-space area $S_1 > 0$ or $S_2 < 0$ in Fig. 1(b). The algebraic sum $S_1 + S_2 = q_x(2\pi\hbar/b)$ depends only on $q_x = (ed/c)B_y$. Constructive interference between $\boldsymbol{k}_1$ and $\boldsymbol{k}_3$ requires that $(S_1 + S_2)c/\hbar eB_z = 2\pi n$, which is equivalent to the Lebed condition $B_y' = n$.

Interference between $\boldsymbol{k}_1$ and $\boldsymbol{k}_2$ is controlled by the area S_1. Introducing the dimensionless variable $S_1' = S_1 c/\hbar eB_z$, we find from Fig. 1(b) that

$$S_1' = 2B_x'\sqrt{1 - \left(\frac{B_y'}{B_x'}\right)^2} + B_y'\left[\pi + 2\arcsin\left(\frac{B_y'}{B_x'}\right)\right]. \quad (10)$$

Constructive interference requires that $S_1' = 2\pi(j + 1/4)$, where j is an integer, and the extra phase $\pi/2$ appears because $\boldsymbol{k}_1$ and $\boldsymbol{k}_2$ are the turning points on the Fermi surface, when viewed along the vector $\boldsymbol{q}$. The lines with circles show where in Fig. 2 this condition is satisfied. Maxima of σ_c are achieved at the circled intersections of these lines and the integer vertical lines, where both S_1 and $S_1 + S_2$ give constructive interference. These points correspond to the maxima of the Bessel functions in Eq. (8). The lines with squares in Fig. 2 show where the interference in S_1 is destructive (j is half-integer). At the intersections of these lines and the integer vertical lines, marked by squares, σ_c has minima, and the Bessel functions in Eq. (8) have zeros. There, $\sigma_c \to 0$ at $\omega_c\tau \to \infty$, and resistivity $\rho_c = 1/\sigma_c$ increases without saturation when $B \to \infty$, whereas $\rho_c(B)$ saturates at the circles [32]. The maxima and minima of σ_c create a checkerboard pattern of oscillations [31] for $|B_x'| > |B_y'|$ in Fig. 2.

The diagonal line $B_x' = B_y'$ in Fig. 2 corresponds to the third angular effect [24–26]. At this line, the points $\boldsymbol{k}_2$ and $\boldsymbol{k}_3$ merge, and the area S_2 shrinks to zero in Fig. 1(b). For $|B_x'| < |B_y'|$, the two Fermi surfaces do not cross in Fig. 1(b), so interlayer tunneling is suppressed, and σ_c does not show oscillations below the diagonal lines in Fig. 2. However, this contradicts experiments [37,38], which show the Lebed oscillations of σ_c vs B_y' at $B_x = 0$.

To improve the theory, let us consider a model with interlayer tunneling amplitudes t_m between the chains shifted by m units in the y direction [30]. The tunneling displacement is $\boldsymbol{d} + m\boldsymbol{b}$, so the phase in Eq. (2) becomes

$$\phi(\boldsymbol{r}) = \frac{e}{\hbar c}(A_z d + A_y m b), \qquad A_y = B_z x. \quad (11)$$

Comparing Eqs. (3) and (11), we see that results in this case can be obtained by substitution $B_y d \to B_y d - B_z m b$ and $B_y' \to B_y' - m$ in the old results. Equation (6) transforms into $\tilde{t}_m = t_m J_{n-m}(B_x')$ for $B_y' = n$, and Eq. (8) becomes

$$\frac{\sigma_c(\boldsymbol{B},\omega)}{\sigma_c(0,0)} = \sum_m \sum_{n=-\infty}^{\infty} \frac{t_m'^2 J_{n-m}^2(B_x')}{1 + (\omega_c\tau)^2(n - B_y' \mp \omega/\omega_c)^2}, \quad (12)$$

where $t_m'^2 = t_m^2/\sum_l t_l^2$. The contour plot of Eq. (12) can be obtained by shifting the plot in Fig. 2 by m units along the B_y' axis and adding the shifted plots with the weights $t_m'^2$. The resulting contour plot, calculated for $t_0 = t_c$, $t_{\pm 1} = t_c/2$, and $t_{\pm 2} = t_c/4$, is shown in Fig. 3. At $B_x = 0$, $\sigma_c(B_y')$ has maxima for those directions $B_y' = m$ where t_m exists [30,33]. Oscillations of σ_c vs B_x' are smeared in Fig. 3, because the shifted maxima and minima of the checkerboard pattern in Fig. 2 add up out of phase. This is illustrated in Fig. 4, which shows that the DKC oscillations of $\sigma_c(B_x')$ for $B_y = 0$ are much weaker for multiple t_m. Moreover, σ_c does not have zeros at $B_y' = n$. Thus, when $B \to \infty$, $\rho_c(B)$ saturates on the integer lines in Fig. 3, but grows without saturation between the lines. Weak DKC oscillations of $\sigma_c(B_x')$ at $B_y = 0$ and strong Lebed oscillations of $\sigma_c(B_y')$ at $B_x = 0$ correspond qualitatively to $(TMTSF)_2PF_6$ [23,37,38], indicating that several t_m are present. The opposite case, strong DKC and weak Lebed oscillations, is found in $(TMTSF)_2ClO_4$ [19,20,22], suggesting that it has only one dominant $t_0 = t_c$ [36]. The model parameters can be determined by quantitative comparison between the calculated plots and experimental data for $\sigma_c(B_x', B_y')$. Figure 3 shows that the strength of the Lebed oscillations in σ_c vs B_y' increases when $B_x' \neq 0$, in agreement with the Lee-Naughton experiment [27].

The amplitudes t_m do not necessarily represent electron overlap between distant chains. They may be effective parameters in a model [39], where $\varepsilon(k_x)$ has curvature, so v_F depends on k_x and varies along the quasiclassical trajectory (4). The resulting expression for σ_c has a form similar to Eq. (12) with some effective parameters t_m, which themselves may depend on $\boldsymbol{B}$ [39].

While Eq. (12) may well describe the oscillatory part of σ_c, it often fails to describe the background, particularly in

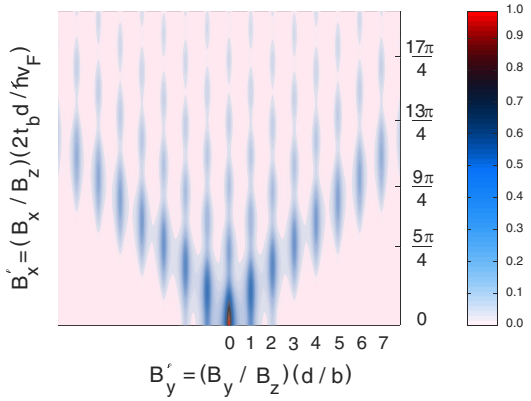

FIG. 3 (color online). Contour plot of the normalized interlayer dc conductivity $\sigma_c(\boldsymbol{B}, 0)/\sigma_c(0, 0)$ vs B_x' and B_y' calculated from Eq. (12). Compared with Fig. 2, this plot takes into account additional tunneling amplitudes t_m along $\boldsymbol{d} + m\boldsymbol{b}$: $t_{\pm 1} = t_c/2$ and $t_{\pm 2} = t_c/4$, which produce the Lebed oscillations at $B_x = 0$.

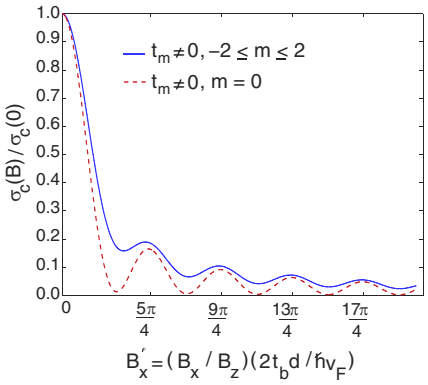

FIG. 4 (color online). Comparison between the normalized interlayer dc conductivities $\sigma_c(\boldsymbol{B}, 0)/\sigma_c(0, o)$ calculated from Eq. (8) (dashed line) and Eq. (12) (solid line) and plotted vs B_x' for $B_y = 0$. The DKC oscillations are reduced in the latter case, because of the additional tunneling amplitudes t_m.

$(TMTSF)_2PF_6$ [23,33,37,38], although there are variations with pressure and sample [40]. This remains one of the open problems, along with unusual temperature dependence of resistivity [37] and mysterious angular oscillations of the Nernst effect [41].

We presented a unified geometrical explanation of different types of AMRO in Q1D conductors in terms of Aharonov-Bohm interference in interlayer electron tunneling. We visualized a two-parameter pattern of oscillations for generic magnetic field orientations using the natural variables B_x' and B_y'. Quantitative comparison with experimental data plotted in this way is needed.

This work was supported by the NSF Grant No. DMR-0137726.

[1] M. V. Kartsovnik *et al.*, JETP Lett. **48**, 541 (1988).
[2] K. Kajita *et al.*, Solid State Commun. **70**, 1189 (1989).
[3] T. Ishiguro, K. Yamaji, and G. Saito, *Organic Superconductors* (Springer, Berlin, 1998).
[4] M. V. Kartsovnik *et al.*, J. Phys. I (France) **2**, 89 (1992).
[5] P. A. Goddard *et al.*, Phys. Rev. B **69**, 174509 (2004).
[6] Y. Iye, M. Baxendale, and V. Z. Mordkovich, J. Phys. Soc. Jpn. **63**, 1643 (1994).
[7] Y. Yoshida *et al.*, J. Phys. Soc. Jpn. **67**, 1677 (1998); **67**, 2551 (1998); E. Ohmichi *et al.*, Phys. Rev. B **59**, 7263 (1999); J. Phys. Soc. Jpn. **68**, 24 (1999).
[8] A. Drăgulescu, V. M. Yakovenko, and D. J. Singh, Phys. Rev. B **60**, 6312 (1999).
[9] N. E. Hussey *et al.*, Nature (London) **425**, 814 (2003).
[10] R. Yagi *et al.*, J. Phys. Soc. Jpn. **60**, 3784 (1991); M. Kawamura *et al.*, Physica B (Amsterdam) **249–251**, 882 (1998); T. Osada, H. Nose, and M. Kuraguchi, *ibid.* **294–295**, 402 (2001).
[11] K. Yamaji, J. Phys. Soc. Jpn. **58**, 1520 (1989).
[12] R. Yagi *et al.*, J. Phys. Soc. Jpn. **59**, 3069 (1990).
[13] Y. Kurihara, J. Phys. Soc. Jpn. **61**, 975 (1992); **62**, 255 (1993); D. Yoshioka, *ibid.* **64**, 3168 (1995).
[14] R. H. McKenzie and P. Moses, Phys. Rev. Lett. **81**, 4492 (1998); P. Moses and R. H. McKenzie, Phys. Rev. B **60**, 7998 (1999); U. Lundin and R. H. McKenzie, *ibid.* **70**, 235122 (2004).
[15] T. Osada *et al.*, Synth. Met. **133–134**, 75 (2003); **135–136**, 653 (2003); Physica E (Amsterdam) **12**, 272 (2002); **18**, 200 (2003).
[16] V. M. Yakovenko and B. K. Cooper, cond-mat/0507120.
[17] G. S. Boebinger, A. Passner, L. N. Pfeiffer, and K. W. West, Phys. Rev. B **43**, 12 673 (1991); N. E. Harff *et al.*, *ibid.* **55**, R13 405 (1997).
[18] A. G. Lebed, JETP Lett. **43**, 174 (1986).
[19] T. Osada *et al.*, Phys. Rev. Lett. **66**, 1525 (1991).
[20] M. J. Naughton *et al.*, Phys. Rev. Lett. **67**, 3712 (1991).
[21] W. Kang, S. T. Hannahs, and P. M. Chaikin, Phys. Rev. Lett. **69**, 2827 (1992).
[22] G. M. Danner, W. Kang, and P. M. Chaikin, Phys. Rev. Lett. **72**, 3714 (1994).
[23] G. M. Danner and P. M. Chaikin, Phys. Rev. Lett. **75**, 4690 (1995).
[24] H. Yoshino *et al.*, J. Phys. Soc. Jpn. **64**, 2307 (1995); **66**, 2248 (1997); **66**, 2410 (1997).
[25] T. Osada, S. Kagoshima, and N. Miura, Phys. Rev. Lett. **77**, 5261 (1996).
[26] A. G. Lebed and N. N. Bagmet, Phys. Rev. B **55**, R8654 (1997).
[27] I. J. Lee and M. J. Naughton, Phys. Rev. B **57**, 7423 (1998).
[28] T. Osada *et al.*, Synth. Met. **103**, 2024 (1999).
[29] H. Yoshino and K. Murata, J. Phys. Soc. Jpn. **68**, 3027 (1999); S. J. Blundell and J. Singleton, Phys. Rev. B **53**, 5609 (1996).
[30] T. Osada, S. Kagoshima, and N. Miura, Phys. Rev. B **46**, 1812 (1992).
[31] A. G. Lebed and M. J. Naughton, Phys. Rev. Lett. **91**, 187003 (2003).
[32] A. G. Lebed, H.-I. Ha, and M. J. Naughton, Phys. Rev. B **71**, 132504 (2005); cond-mat/0503649.
[33] E. I. Chashechkina and P. M. Chaikin, Phys. Rev. B **65**, 012405 (2002).
[34] V. M. Yakovenko and H.-S. Goan, Phys. Rev. B **58**, 8002 (1998).
[35] A. Ardavan *et al.*, Phys. Rev. Lett. **81**, 713 (1998); A. E. Kovalev, S. Hill, and J. S. Qualls, Phys. Rev. B **66**, 134513 (2002); Y. Oshima *et al.*, *ibid.* **68**, 054526 (2003).
[36] S. Takahashi *et al.*, Phys. Rev. B **72**, 024540 (2005).
[37] E. I. Chashechkina and P. M. Chaikin, Phys. Rev. Lett. **80**, 2181 (1998).
[38] D. G. Clarke, S. P. Strong, P. M. Chaikin, and E. I. Chashechkina, Science **279**, 2071 (1998).
[39] K. Maki, Phys. Rev. B **45**, R5111 (1992); A. G. Lebed, N. N. Bagmet, and M. J. Naughton, Phys. Rev. Lett. **93**, 157006 (2004).
[40] I. J. Lee and M. J. Naughton, Phys. Rev. B **58**, R13343 (1998); H. Kang, Y. J. Jo, and W. Kang, *ibid.* **69**, 033103 (2004).
[41] W. Wu, I. J. Lee, and P. M. Chaikin, Phys. Rev. Lett. **91**, 056601 (2003); N. P. Ong, W. Wu, P. M. Chaikin, and P. W. Anderson, Europhys. Lett. **66**, 579 (2004); W. Wu, N. P. Ong, and P. M. Chaikin, Phys. Rev. B **72**, 235116 (2005). E. S. Choi *et al.*, Phys. Rev. Lett. **95**, 187001 (2005).